Exchange-split interface state at h-BN/Ni(111)

Karen Zumbrägel, Kathrin Wulff, Christian Eibl, and Markus Donath
Physikalisches Institut, Westfälische Wilhelms-Universität, Wilhelm-Klemm-Strasse 10, 48149 Münster, Germany

Matthias Hengsberger
Physics Institute of the University of Zürich, Winterthurerstrasse 190, 8057 Zürich, Switzerland
(Received 12 June 2008; published 19 August 2008)

The insulator/ferromagnet interface system of hexagonal boron nitride on Ni(111) was investigated with spin- and angle-resolved inverse photoemission and spin-polarized secondary electron emission. We identified the theoretically predicted boron nitride (BN) interface state at 1.7 eV above the Fermi level. The interface state is found to be influenced by the ferromagnetic substrate, which is reflected in a magnetic exchange splitting of 130 ± 50 meV. Parallel to the surface, it shows a free-electron-like $E(\mathbf{k}_{\parallel})$ dispersion with an effective mass of $1.1 \pm 0.2 m_e$. Furthermore, we found a spectral feature at 2.2 eV above the Fermi level, which we attribute to indirect transitions into a region of high density of BN-induced states.

DOI: 10.1103/PhysRevB.78.085422 PACS number(s): 75.70.Cn, 79.60.Dp, 73.20.−r, 73.40.Ns

I. INTRODUCTION

Insulator/ferromagnet interfaces play a major role in electronic devices for information storage technology and have, consequently, sparked considerable scientific interest.[1] The application potential of a device hinges on characteristic material properties such as the electrical conductivity or the magnetization, which in turn are determined by the electronic states around the Fermi energy E_F.

A model system is hexagonal boron nitride on the (111) surface of nickel: h-BN/Ni(111). The electronic properties of the constituent parts, the (111) surface of the $3d$ band ferromagnet nickel,[2–8] and the chemically inert insulator boron nitride[9–11] (BN) have already been thoroughly explored. h-BN/Ni(111) was further employed as a substrate for the investigation of C_{60} molecules because the h-BN layer electronically decouples the molecules from the substrate.[12] In recent years, various experimental[13–15] and theoretical studies[16,17] were performed on the interface h-BN/Ni(111) to investigate the atomic arrangement as well as the electronic structure. Auwärter *et al.*[13] characterized the atomic configuration of h-BN/Ni(111) with scanning tunneling microscopy (STM). Their results agree with calculations by Grad *et al.*[16] and Huda and Kleinman:[17] The nitrogen atoms are located directly on top of the nickel atoms of the outermost layer. The positions of the boron atoms correspond to the positions of the third layer nickel atoms.

In addition to the geometric structure, the electronic band structure $E(\mathbf{k}_{\parallel})$ was calculated above and below the Fermi level along the main symmetry directions within the fcc (111) surface plane. The lowest-lying conduction band above the Fermi level originating from the BN layer is called an interface band because its states are localized between the nickel substrate and the BN overlayer. For this interface band, Grad *et al.*[16] predict an energetic position between 1.50 and 1.76 eV above the Fermi energy at $\bar{\Gamma}$, a free-electron-like $E(\mathbf{k}_{\parallel})$ dispersion, and an exchange splitting in the range of 130 meV.

Nagashima *et al.*[18,19] investigated the occupied band structure with angle-resolved ultraviolet-photoelectron spectroscopy (ARUPS) and the unoccupied electronic states above the vacuum level with angle-resolved secondary-electron-emission spectroscopy (ARSEES). The results of the band structure below the Fermi energy confirm the calculations but the lowest conduction band was found at an energy of 2.7 eV above E_F, in contrast to the theoretical prediction.[16] More recent ARUPS results for the occupied bands are again in agreement with the calculations.[16]

The unoccupied part of the band structure between the Fermi energy and the vacuum level was investigated with two-photon photoemission (2PPE) by Muntwiler *et al.*[20] For the interface state, they determined an energetic position of 1.51 eV and an effective mass of $0.43 \pm 0.1 m_e$.

In the present study, our focus of interest is the exchange splitting of the unoccupied interface state. Therefore, we performed angle- and spin-resolved inverse-photoemission (IPE) measurements on h-BN/Ni(111). We determined the energetic position of the interface state, its $E(\mathbf{k}_{\parallel})$ dispersion, and its dependence on the electron spin. For a meaningful interpretation of the data, it was necessary to carefully characterize the remanent magnetization of the Ni(111) substrate with spin-polarized secondary electron emission (SPSEE). It turned out that the remanent magnetization equals the saturation magnetization only for temperatures above about 350–400 K, corresponding to a reduced temperature $T/T_C \approx 0.6$ (T_C Curie temperature, 631 K for bulk nickel). This is a consequence of the temperature-dependent magnetocrystalline anisotropy within the nickel substrate.

II. EXPERIMENT

The measurements were carried out in an ultrahigh vacuum (UHV) system at a base pressure below 10^{-10} mbar. The nickel substrate is a hexagon-shaped picture-frame single crystal with legs along ⟨110⟩ directions and a ⟨111⟩ direction perpendicular to the hexagon plane.[5] The surface under investigation has a (111) orientation. A self-supporting coil with four turns is wound around one leg to magnetize the sample via a current pulse. By doing this, we try to achieve a remanent in-plane magnetization of the Ni frame

along ⟨110⟩ directions. Note that, at room temperature, the axis of easy magnetization in nickel is along ⟨111⟩. However, no ⟨111⟩ direction lies in the surface plane of a crystal with (111) surface orientation. We come back to this point later.

The Ni(111) surface was cleaned by sputter and anneal cycles using 1.2 keV Ar^+ ions and an annealing temperature of 950 K. For the preparation of a h-BN overlayer, the Ni(111) substrate was subsequently heated to 1050 K and borazine vapor $(HBNH)_3$ was introduced into the chamber via a leak valve. At this high temperature, borazine reacts with the hot Ni(111) surface and one monolayer of hexagonal BN is formed on the substrate. A detailed description of the preparation can be found in the literature.[19]

The quality of the preparation was controlled by measuring the work function Φ with target current spectroscopy. Compared with the work function of 5.35 eV for clean Ni(111), the work function is found to be reduced by 1.8 ± 0.1 eV for the h-BN-covered Ni surface. This is in good agreement with previous experimental and theoretical values.[16,20] The long-range crystallographic order of substrate and overlayer was checked with low-energy electron diffraction (LEED). In both cases, the LEED pattern showed sharp diffraction spots of hexagonal order, indicating the crystalline quality of the substrate and the BN monolayer.

The unoccupied states were investigated by spin- and angle-resolved inverse photoemission.[5,21–24] A GaAs photocathode irradiated by circularly polarized laser light is used as a source for spin-polarized electrons.[25,26] The spin polarization of the electron beam is $P_e = 33 \pm 3\%$.[23,27] The electrons impinge on the sample with well defined energy, momentum, and spin polarization. Within the sample, they undergo radiative transitions from initial states above the vacuum level into unoccupied states above the Fermi level. The emitted photons are detected by Geiger-Müller counters in the isochromat mode.[28] The detection energy of the counters (9.4 eV) is determined by the filling gas iodine, acting as high-pass filter, and a window of SrF_2, acting as low-pass filter. The width of the energetic bandpass of the detector and, as a consequence, the mean detection energy can be varied with the temperature of the SrF_2 filter.[28–30] Thus the total energy resolution of the IPE system, which is determined by the electron energy distribution and the detector bandpass width, then can be improved from 0.4 to 0.3 eV full width at half maximum, yet at the cost of reduced count rates. Therefore, the improved energy resolution was only used in cases, where additional information can be obtained from high-resolution measurements. The photons are detected with two counters GM_{35} and GM_{70} at takeoff angles with respect to the incident electron beam of 35° and 70°, respectively. Using two counters with different detection angles gives us the possibility to investigate the radiation pattern of a transition. This information allows conclusions about the symmetry character of the participating states. In the current setup, only GM_{70} is equipped with a heatable SrF_2 window for improved energy resolution.

IPE spectra display the number of photons detected at a given electron energy as a function of the energy of the incoming electrons. The energy scale is referred to the Fermi level of the sample. In the spin-resolved mode, two IPE spectra are measured for opposite spin-polarization directions. The measured numbers of counts $n_\uparrow$ and $n_\downarrow$ for the two different spin-polarization directions are normalized to hypothetical 100% spin polarization of the incoming beam $(N_\uparrow, N_\downarrow)$ with the following equation:

$$N_{\uparrow,\downarrow} = \frac{n_\uparrow + n_\downarrow}{2} \pm \frac{n_\uparrow - n_\downarrow}{2} \frac{1}{P_{\text{eff}}}. \quad (1)$$

P_{eff} denotes the effective spin polarization of the incident electrons. P_{eff} only equals P_e for collinear alignment of electron-spin polarization and sample magnetization. It may be reduced by two effects: (i) non-normal incidence of the incoming electrons (angle θ) and (ii) magnetic domains in remanence within the sample with magnetization directions noncollinear with the electron-spin polarization. P_{eff} is given by

$$P_{\text{eff}} = P_e \cos\theta \, M_r/M_s,$$

where the sample magnetization in remanence and in saturation is denoted by M_r and M_s, respectively.

In order to determine the remanent sample magnetization, we performed measurements with spin-polarized secondary electron emission. The sample is irradiated with an electron beam of 3 keV kinetic energy at an angle of 35° with respect to the surface normal. The spin polarization of the emitted low-energy secondary electrons is determined with a 25 keV retarding-field Mott detector based on the Rice design.[31,32] A thin gold foil is used as scatter target. Electron gun and spin-polarization detector enclose an angle of 70°. The lens voltages of the transfer electron optics are set in such a way that only electrons with energies lower than 10 eV arrive at the Au foil.[27] The scattering asymmetry A_s is measured by a pair of channeltrons a and b and is defined by

$$A_s = \frac{N_a - N_b}{N_a + N_b}.$$

The magnetization direction of the sample was reversed several times during a measurement. Instrumental asymmetries due to different channeltron sensitivities are omitted by taking the geometrical mean of the corresponding numbers of counts.[33] The Sherman function S of our spin-polarization detector was determined to $15 \pm 3\%$ by measuring the scattering asymmetry A_s of an electron beam of known polarization. The spin polarization of the secondary electrons P_s was determined by using $P_s = A_s/(S \cos 35°)$. The cosine factor takes into account the non-normal-emission geometry for the secondary electrons. It was experimentally found that the polarization P_s of the secondary electrons is proportional to the magnetization of the sample.[34] Although P_s cannot be translated quantitatively into a sample magnetization, it gives a measure of the remanent sample magnetization as a function of, e.g., the sample temperature. By this, it provides valuable information about possible magnetization changes, for example, caused by domain formation due to temperature-dependent changes in the magnetocrystalline anisotropy. This information is essential for interpreting the spin-resolved IPE data, whose analysis is usually based on the assumption that the sample is magnetically saturated in remanence.

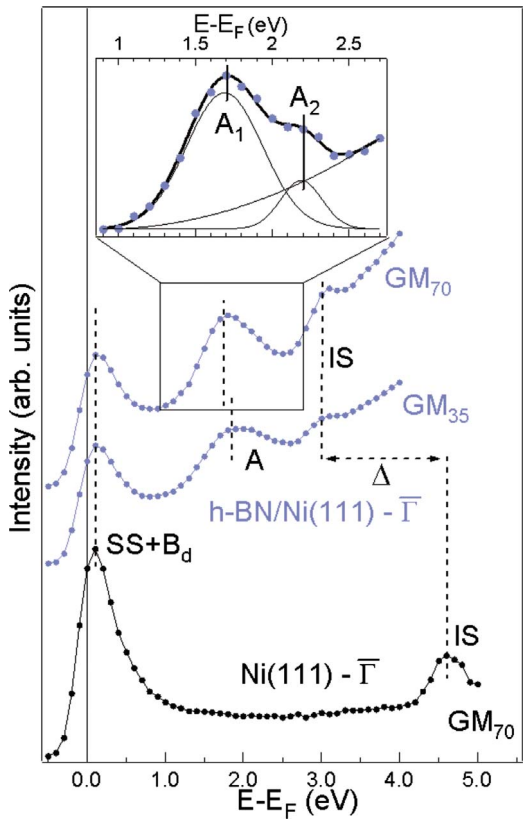

FIG. 1. (Color online) Inverse-photoemission spectra for normal electron incidence (θ=0°) on uncovered Ni(111) detected with GM_{70} (black dots) and on h-BN/Ni(111) detected with GM_{35} and GM_{70} (blue dots). Peak positions are marked by dashed lines. The spectral features just above E_F consist of contributions from a surface state (*SS*) and transitions into bulk *d* states (B_d). *A* denotes the spectral intensity originating from the boron-nitride-induced interface state. Δ indicates the energy shift of the image-potential surface state *IS* between the clean and BN-covered surface. Inset: Inverse-photoemission spectra with improved energy resolution for h-BN/Ni(111) obtained with GM_{70}. The thin lines demonstrate the decomposition of the spectrum into two spectral features A_1 and A_2 plus background intensity.

III. ENERGY DISPERSION

Figure 1 presents our IPE spectra for normal electron incidence on uncovered Ni(111) and h-BN/Ni(111). The spectrum for clean Ni(111) (black dots) shows two dominant peaks. The peak at 0.1 eV above E_F originates from a crystal-induced surface state (*SS*) and from indirect transitions into bulklike Ni *d* bands (B_d).[4] The spectral feature at 4.6 eV is caused by the n=1 member of a Rydberg-like series of image-potential surface states (*IS*).[3] They are pinned to the vacuum level E_{vac}.[35,36] The binding energy of *IS* defined by the difference between the vacuum level (Φ=5.35 eV) and the final-state energy is determined to 0.75 eV, which is in good agreement with previous results.[2,37]

In the two spectra from h-BN/Ni(111) three structures are clearly visible: (i) The peak just above E_F known from the clean surface appears with reduced intensity. (ii) The image-potential surface state shows up at 3.0 eV. The lower final-state energy compared with the clean surface is mainly caused by the BN-induced work-function change. The difference in final-state energy of 1.6 eV is lower than the work-function difference of 1.8 eV between the clean surface and the h-BN-covered surface. This indicates an about 0.2 eV reduced binding energy of *IS* for the BN-covered surface. For comparison, 2PPE data point at a change in binding energy of 0.15 eV.[20,37] As expected for transitions into image-potential states, the dipolar axis is perpendicular to the surface resulting in more intensity in GM_{70} than in GM_{35}.[38] (iii) At about 1.8 eV, a new structure *A* appears in the h-BN/Ni(111) spectra, which we attribute to the predicted interface state of the h-BN/Ni(111) system. It is conspicuous that the shape and the energetic position of *A* differ in the two spectra obtained with different photon takeoff angles. In the spectrum of GM_{35}, the shape of *A* is broader than in the spectrum of GM_{70}, while *A* appears with higher intensity in the latter. Furthermore, the energetic positions of *A* differ by about 0.1 eV for the two different detection geometries: 1.75 eV for GM_{70} and 1.85 eV for GM_{35}. A straightforward explanation for the observed behavior is that the structure contains two transitions in different final states showing different characteristic radiation patterns.[39] To verify this assumption, we performed IPE measurements (GM_{70}) with improved energy resolution in the relevant energy range. The results are shown in the inset of Fig. 1. Clearly, structure *A* consists of two components: A_1 at 1.7 eV and A_2 at 2.2 eV. Based on the energetic position, A_1 is assigned to the expected interface state, while the origin of A_2 is *a priori* not clear. Former experiments with two-photon photoemission identified interface-related states at an energy comparable to A_2 but no clear-cut interpretation could be derived from the measurements.[20]

In the following, we present a detailed investigation of structure *A* with the objective of extracting the different contributions of *A*. We recorded a series of spectra for varying angles of electron incidence along the $\bar{\Gamma}\bar{K}$ direction of the crystal, i.e., the $[1\bar{1}0]$ direction shown in Fig. 2. The spectra give information about the $E(\mathbf{k}_{\parallel})$ dispersion of the interface state and provide further evidence for the existence of a second feature A_2. For example, in the spectrum for θ=−4° taken with GM_{35}, *A* has a shoulder above 2 eV. No doubt about two contributions to *A* continues to exist on the basis of the spectrum for θ=22° for GM_{70}, where the two peaks are clearly separated.

The angle-resolved results can be understood in terms of a strongly dispersing and a nondispersing contribution, which coincide in energy for certain angles. This results in an enhanced spectral intensity for these angles. A_2, the nondispersing part, is located at 2.2 eV as clearly seen for three angles θ=−4°, 0°, 22° in the spectra for both counters. A_1 disperses to higher energies with increasing θ. Because of the higher intensity of A_1 compared with A_2, the dispersion of A_1 is clearly visible. At angles, where A_1 and A_2 coincide in energy, it is difficult to determine exactly their energy positions. For a careful analysis, we fitted the structure with two Gaussian peaks on top of a quadratic background for all angles of electron incidence. The left-hand panel of Fig. 3

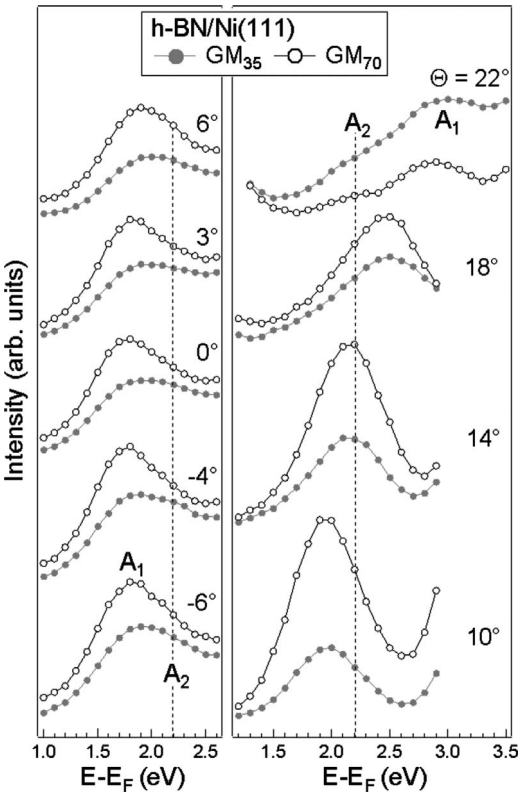

FIG. 2. Inverse-photoemission spectra of structure A as a function of the angle of electron incidence θ. The filled and open symbols represent our data obtained with GM_{35} and GM_{70}, respectively. The spectra are vertically offset for reasons of clarity. Vertical dashed lines mark a final-state energy of 2.2 eV.

shows an example for $\theta=6°$ and for both counters. For reasons of comparison, we fitted the spectrum with only one Gaussian peak as well, shown in the right-hand panel of Fig.

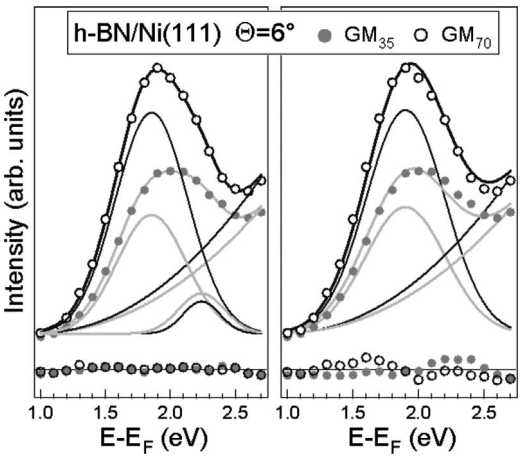

FIG. 3. Inverse-photoemission spectra of h-BN/Ni(111) for $\theta=6°$ obtained with GM_{35} (filled dots) and GM_{70} (open dots). The solid black (for GM_{70}) and gray lines (for GM_{35}) represent decompositions of the spectra into two Gaussian peaks (left-hand panel) and one Gaussian peak (right-hand panel) on top of a quadratic background, respectively. The quality of the fits can be evaluated from the lines through the data points and from the difference between fit and data points as given in the bottom part of the figure.

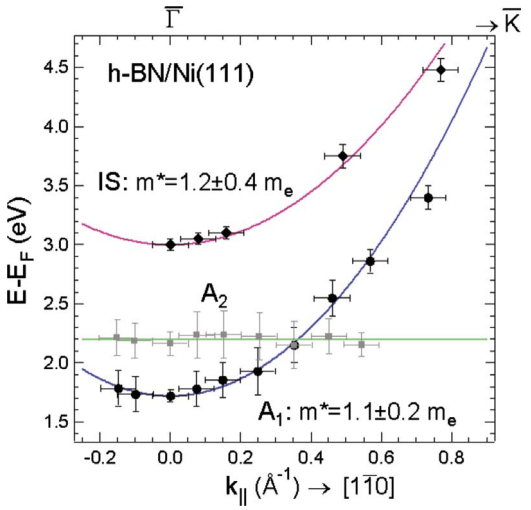

FIG. 4. (Color online) $E(\mathbf{k}_{\|})$ dispersion for the BN-induced states A_1 and A_2 and the image-potential state *IS* as derived from the spectra of Fig. 2.

3. In the upper part of the figure, we present the data points, the different contributions to the fit, and the total fit. In the lower part, the difference between fit and data points is displayed for evaluation of the quality of the fit. A random scatter of the difference around the zero line indicates a good fit, while systematic deviations indicate deficiencies of the fit. It is obvious that two Gaussians are needed for a sufficiently good fit. Based on this analysis, we conclude that A consists of two contributions. In the same way, we determined the energetic positions of A_1 and A_2 for the various angles of electron incidence with the side condition that, for a given angle, the states appear at the same energies for the two counters. Needless to say, the error bars are larger for angles of incidence, where both spectral contributions are not well separated.

Our results for the BN-induced states A_1 and A_2 and the image-potential state *IS* are summarized in Fig. 4 as $E(\mathbf{k}_{\|})$ diagram. A_1 and *IS* exhibit a parabolic free-electron-like dispersion with effective masses of $1.1\pm0.2m_e$ and $1.2\pm0.4m_e$, respectively, while A_2 shows no dispersion as a function of $\mathbf{k}_{\|}$. As both the energetic position at $\bar{\Gamma}$ and the free-electron-like dispersion $E(\mathbf{k}_{\|})$ of A_1 agree with the theoretical prediction by Grad *et al.*,[16] we identify A_1 as the interface state. We have to note that our result of the effective mass does not agree with the effective mass of $0.43\pm0.1m_e$ measured by Muntwiler *et al.*[20] We can only speculate about the origin of this difference. In the 2PPE process, three states are involved (initial, intermediate, and final state), whereas only two states (initial and final state) participate in the IPE process. Because of the additional state in 2PPE, various excitation channels exist and interact. As a consequence it may prove more difficult to unambiguously assign the energetic position of an intermediate state.

The feature A_2 shows no dispersion. A similar peak at 2.2 eV above E_F was observed by means of two-photon photoemission and was attributed to the second state of a series of interface states,[20] which have been predicted from earlier density-functional calculations.[11] In contrast to the predicted

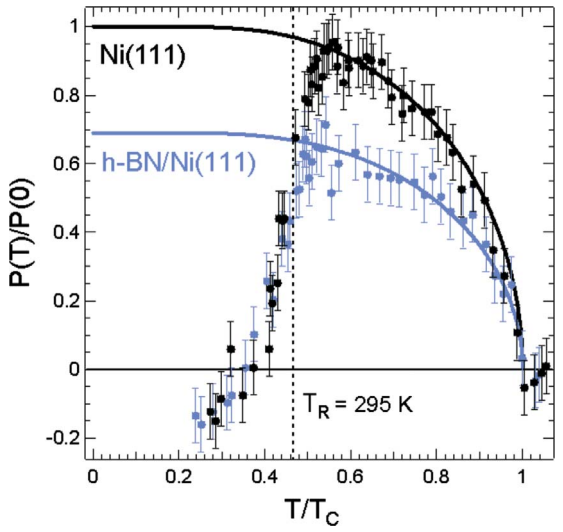

FIG. 5. (Color online) Spin-polarized secondary electron emission measurements as a function of the temperature for clean Ni(111) (black dots) and h-BN/Ni(111) (blue dots). The solid lines represent the saturation magnetization $M(T)$ of bulk Ni, described by Weiss' theory, fitted to the data points for temperatures above $T/T_C=0.6$. Room temperature T_R is marked by a dashed vertical line.

free-electron-like dispersion of such states, we did not observe any dispersion of the peak as a function of the momentum parallel to the surface. Therefore, we tend to assign the observed dispersionless feature A_2 to indirect transitions into a region of high density of BN-induced states at the $\bar{K}$ point corresponding to flat bands at about 2 eV.[16]

IV. MAGNETIC EXCHANGE SPLITTING

After having determined the energy dispersion of the interface state, we investigated the influence of the ferromagnetic substrate by a spin-resolved inverse-photoemission experiment. To get reliable and quantitative results from spin-polarized electron spectroscopies on ferromagnets, an essential requirement has to be met. The angle between the directions of the electron-spin polarization and sample magnetization has to be well defined. In our case, the direction of the electron-spin polarization is given by the geometry of the experiment. For measurements with normal electron incidence, our setup is sensitive to one in-plane component of the magnetization. We need a sample which is magnetically saturated in remanence parallel to the surface plane and collinear with the electron-spin polarization. However, as mentioned before, the Ni(111) surface contains no axes of easy magnetization in the surface plane at room temperature. Yet, our particular hexagon-shaped single crystal with its individual history had already been used in former studies with a surprising property: It was found to be remanently magnetized in the surface plane in a metastable one-domain state.[3,5] Therefore, we were expecting the same behavior in the present study. We were surprised to find a significantly smaller spin asymmetry in the IPE data from clean Ni(111) compared with former results.[3]

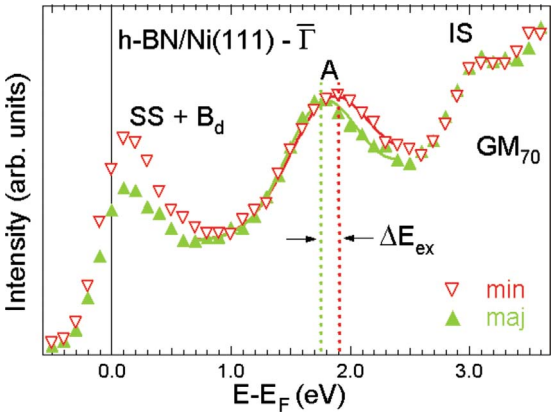

FIG. 6. (Color online) Spin-resolved inverse-photoemission spectrum for normal electron incidence on h-BN/Ni(111), detected with GM_{70}. The solid (green) and open (red) triangles represent the IPE data for majority and minority spins, respectively. The data were obtained at room temperature and the spin asymmetry was rescaled according to Fig. 5. The solid lines were obtained from Gaussian line fits to the data. The spin-dependent peak positions for A are marked by dashed lines.

To shed more light on this issue, we tested the surface magnetization M as a function of the temperature by measuring the spin polarization of emitted low-energy secondary electrons. Our data for the clean Ni(111) surface as well as the BN-covered surface are shown in Fig. 5. With the proportionality $P(T)\sim M(T)$ in mind, both data sets show a typical $M(T)$ dependence for temperatures higher than $T/T_C=0.6$, yet with reduced absolute values for the BN-covered surface. The solid lines represent the temperature dependence of the nickel bulk magnetization, described by Weiss' theory, fitted to the respective data sets for temperatures higher than about $T/T_C=0.6$. For lower temperatures, the data points deviate substantially from the expected $M(T)$ behavior. They even become negative for temperatures below $T/T_C=0.4$. Qualitatively, the same behavior had been observed for Ni(001) and explained by the change of magnetocrystalline anisotropy in Ni at about $T/T_C=0.6$ from $\langle 111\rangle$ to $\langle 110\rangle$ as axes of easy magnetization.[40,41] The unexpectedly small spin-polarization values for lower T are a consequence of the formation of magnetic closure domains in the surface region. The results presented in Fig. 5 lead us to the following conclusions.

(i) The surface magnetization of Ni(111) and h-BN/Ni(111) shows qualitatively the same temperature dependence, yet with absolute values reduced by about 30%. The reduction of spin polarization is caused by adsorption of the nonmagnetic insulating monolayer. On the one hand, a reduced magnetic moment of Ni at the BN interface is theoretically espected.[16] On the other hand, the secondary electrons become depolarized upon passing the BN layer. No influence of the BN layer on the magnetic structure within the Ni is detected. Recently, the isoelectronic system of graphene on Ni(111) was investigated by SPSEE. Similarly, a 30% reduction of the spin polarization was detected upon adsorption.[42]

(ii) Our picture-frame single crystal is no longer in a one-domain state when remanently magnetized. The numerous

preparation sputter/anneal cycles presumably helped to reduce the strain/stress-induced anisotropy responsible for the formerly observed one-domain state in remanence. As a consequence, quantitative measurements with spin-resolved electron spectroscopies have to be performed either at elevated temperatures above $T/T_C=0.6$ or have to be rescaled on the basis of the $P(T)$ data in Fig. 5. Both approaches gave equivalent results.

Spin-resolved inverse-photoemission data for normal electron incidence on h-BN/Ni(111) at room temperature obtained with GM_{70} are presented in Fig. 6. The photon intensity is plotted as a function of the electron energy with respect to the Fermi level for two spin orientations either parallel or antiparallel to the magnetization direction of the sample. This provides access to minority and majority states within the ferromagnetic sample. The data have been normalized according to Eq. (1), whereas P_{eff} includes the incomplete remanent surface magnetization as given in Fig. 5. The solid (open) triangles denote IPE data for majority (minority) electrons, which means that the spin magnetic moment of the incoming electrons is parallel (antiparallel) to the sample magnetization. Compared with the clean surface, a reduced intensity is observed in both spin channels for the structure just above E_F. The BN-induced feature A appears at different final-state energies for majority and minority electrons. It exhibits a clear magnetic exchange splitting ΔE_{ex} of 130 ± 50 meV. The considerable error margins reflect the uncertainty in the rescaling factor due to the large slope around room temperature in the data of Fig. 5. From Fig. 1 we know that A is dominated by A_1 in the spectrum obtained with GM_{70}. Therefore, ΔE_{ex} reflects predominantly the exchange splitting of A_1.

The value of the exchange splitting is in good agreement with the theoretical prediction of $\approx$130 meV by Grad *et al.*[16] The size of the splitting is comparable with surface-state exchange splittings on clean Ni surfaces.[4,5] Our result proves the strong influence of the ferromagnetic substrate on the interface state. However, theory expects a reduced magnetic moment for the outermost Ni layer when covered by BN. As a strong ferromagnet, Ni has no empty majority d states. A reduced magnetic moment may be reflected in majority holes giving rise to majority intensity just above E_F. The interpretation of the observed majority intensity is, however, not straightforward because, on the clean surface, the majority intensity is caused by a crystal-induced surface state whose whereabout upon adsorption is not clear.

V. SUMMARY

We performed a detailed spin- and angle-resolved inverse-photoemission study of the insulator/ferromagnet interface system of h-BN/Ni(111). We identified interface-induced electron states and determined their energy dispersion as a function of the momentum parallel to the surface. A theoretically predicted interface state A_1 was detected at 1.7 eV above the Fermi energy. It shows a free-electron-like dispersion with an effective mass of $1.1\pm0.2m_e$. A second BN-induced structure A_2 at 2.2 eV above the Fermi energy shows no $E(\mathbf{k}_{\parallel})$ dispersion. We assign A_2 to indirect transitions into a region of high density of BN-induced states at the $\bar{K}$ point.

Quantitative measurements with spin resolution are based on a thorough analysis of the remanent surface magnetization of Ni(111) as a function of the temperature by spin-polarized secondary electron emission. Our data confirm a temperature-dependent change of the magnetocrystalline anisotropy of bulk nickel. As a consequence, magnetic surface domains are formed in remanence for temperatures below $T/T_C=0.6$. Our results reveal a magnetic exchange splitting of 130 ± 50 meV for the BN-induced interface state. The size of the splitting reveals a strong influence of the ferromagnetic substrate on the interface state.

ACKNOWLEDGMENTS

We gratefully acknowledge Thomas Greber for initiating the collaboration and for valuable discussions. We thank M. Kloeckner for technical assistance with the setup of the borazine source and H. Sachdev for providing the borazine.

[1] S. Gider, B.-U. Runge, A. C. Marley, and S. S. P. Parkin, Science **281**, 797 (1998).
[2] A. Goldmann, M. Donath, W. Altmann, and V. Dose, Phys. Rev. B **32**, 837 (1985).
[3] F. Passek and M. Donath, Phys. Rev. Lett. **69**, 1101 (1992).
[4] M. Donath, F. Passek, and V. Dose, Phys. Rev. Lett. **70**, 2802 (1993).
[5] M. Donath, Surf. Sci. Rep. **20**, 251 (1994).
[6] J. Kutzner, R. Paucksch, C. Jabs, H. Zacharias, and J. Braun, Phys. Rev. B **56**, 16003 (1997).
[7] T. J. Kreutz, T. Greber, P. Aebi, and J. Osterwalder, Phys. Rev. B **58**, 1300 (1998).
[8] M. Higashiguchi, K. Shimada, M. Arita, Y. Miura, N. Tobita, X. Cui, Y. Aiura, H. Namatame, and M. Taniguchi, Surf. Sci. **601**, 4005 (2007).
[9] A. Catellani, M. Posternak, A. Baldereschi, and A. J. Freeman, Phys. Rev. B **36**, 6105 (1987).
[10] S. P. S. Arya and A. D'Amico, Thin Solid Films **157**, 267 (1988).
[11] X. Blase, A. Rubio, S. G. Louie, and M. L. Cohen, Phys. Rev. B **51**, 6868 (1995).
[12] M. Muntwiler, W. Auwärter, A. P. Seitsonen, J. Osterwalder, and T. Greber, Phys. Rev. B **71**, 121402(R) (2005).
[13] W. Auwärter, T. J. Kreutz, T. Greber, and J. Osterwalder, Surf. Sci. **429**, 229 (1999).
[14] Y. Gamou, M. Terai, A. Nagashima, and C. Oshima, Sci. Rep. Res. Inst. Tohoku Univ. A **44**, 211 (1997).
[15] M. Muntwiler, W. Auwärter, F. Baumberger, M. Hoesch, T. Greber, and J. Osterwalder, Surf. Sci. **472**, 125 (2001).
[16] G. B. Grad, P. Blaha, K. Schwarz, W. Auwärter, and T. Greber, Phys. Rev. B **68**, 085404 (2003).
[17] M. N. Huda and L. Kleinman, Phys. Rev. B **74**, 075418 (2006).

[18] A. Nagashima, N. Tejima, Y. Gamou, T. Kawai, and C. Oshima, Phys. Rev. Lett. **75**, 3918 (1995).
[19] A. Nagashima, N. Tejima, Y. Gamou, T. Kawai, and C. Oshima, Phys. Rev. B **51**, 4606 (1995).
[20] M. Muntwiler, M. Hengsberger, A. Dolocan, H. Neff, T. Greber, and J. Osterwalder, Phys. Rev. B **75**, 075407 (2007).
[21] V. Dose, Surf. Sci. Rep. **5**, 337 (1985).
[22] N. V. Smith, Rep. Prog. Phys. **51**, 1227 (1988).
[23] M. Donath, Appl. Phys. A: Solids Surf. **49**, 351 (1989).
[24] M. Donath, J. Phys.: Condens. Matter **11**, 9421 (1999).
[25] D. T. Pierce and F. Meier, Phys. Rev. B **13**, 5484 (1976).
[26] U. Kolac, M. Donath, K. Ertl, H. Liebl, and V. Dose, Rev. Sci. Instrum. **59**, 1933 (1988).
[27] D. Yu, C. Math, M. Meier, M. Escher, G. Rangelov, and M. Donath, Surf. Sci. **601**, 5803 (2007).
[28] V. Dose, Th. Fauster, and R. Schneider, Appl. Phys. A: Solids Surf. **40**, 203 (1986).
[29] J. Braun, C. Math, A. Postnikov, and M. Donath, Phys. Rev. B **65**, 184412 (2002).
[30] M. Budke, V. Renken, H. Liebl, G. Rangelov, and M. Donath, Rev. Sci. Instrum. **78**, 083903 (2007).
[31] F. B. Dunning, L. G. Gray, J. M. Ratliff, F.-C. Tang, X. Zhang, and G. K. Walters, Rev. Sci. Instrum. **58**, 1706 (1987).
[32] G. C. Burnett, T. J. Monroe, and F. B. Dunning, Rev. Sci. Instrum. **65**, 1893 (1994).
[33] J. Kessler, *Polarized Electrons*, Springer Series on Atoms and Plasmas Vol. 1, 2nd ed. (Springer, Berlin, 1985).
[34] M. Landolt, Appl. Phys. A: Solids Surf. **41**, 83 (1986).
[35] P. M. Echenique and J. B. Pendry, J. Phys. C **11**, 2065 (1978).
[36] P. M. Echenique and M. E. Uranga, Surf. Sci. **247**, 125 (1991).
[37] S. Schuppler, N. Fischer, W. Steinmann, R. Schneider, and E. Bertel, Phys. Rev. B **42**, 9403 (1990).
[38] V. Dose, W. Altmann, A. Goldmann, U. Kolac, and J. Rogozik, Phys. Rev. Lett. **52**, 1919 (1984).
[39] M. Donath, M. Glöbl, B. Senftinger, and V. Dose, Solid State Commun. **60**, 237 (1986).
[40] K. Starke, K. Ertl, and V. Dose, Phys. Rev. B **46**, 9709 (1992).
[41] G. Aubert, J. Appl. Phys. **39**, 504 (1968).
[42] Y. S. Dedkov, M. Fonin, and C. Laubschat, Appl. Phys. Lett. **92**, 052506 (2008).